A molecular-dynamics study of structural and physical properties of nitromethane nanoparticles

ARTICLE *in* THE JOURNAL OF CHEMICAL PHYSICS · JULY 2004

Impact Factor: 2.95 · DOI: 10.1063/1.1730074 · Source: PubMed

A molecular-dynamics study of structural and physical properties of nitromethane nanoparticles

Saman Alavi[a] and Donald L. Thompson[b]
Department of Chemistry, Oklahoma State University, Stillwater, Oklahoma 74078

(Received 2 September 2003; accepted 9 March 2004)

The structural and physical properties of nanoparticles of nitromethane are studied by using molecular dynamics methods with a previously developed force field. [Agrawal *et al.*, J. Chem. Phys. **119**, 9617 (2003).] This force field accurately predicts solid- and liquid-state properties as well as melting of bulk nitromethane. Molecular dynamics simulations of nanoparticles with 480, 240, 144, 96, 48, and 32 nitromethane molecules have been carried out at various temperatures. The carbon–carbon radial distribution function, dipole–dipole correlation function, core density, internal enthalpy, and atomic diffusion coefficients of the nanoparticles were calculated at each temperature. These properties were used to characterize the physical phases and thus determine the melting transitions of the nanoparticles. The melting temperatures predicted by the various properties are consistent with one another and show that the melting temperature increases with particle size, approaching the bulk limit for the largest particle. A size dependence of melting points has been observed in experimental and theoretical studies of atomic nanoparticles, and this is a further demonstration of the effect for large nanoparticles of complex molecular materials. © *2004 American Institute of Physics.* [DOI: 10.1063/1.1730074]

I. INTRODUCTION

Nanoparticles which are aggregates of about $10-10^6$ atoms or molecules have diameters ranging for 1–100 nm, have been the subject of much study in recent years.[1,2] Theoretical and experimental studies of nanoparticles of model Lennard-Jones particles,[3–5] metals,[6–13] semiconductor materials such as CdS,[14,15] water,[16–18] metallic oxides,[19,20] CO_2,[21] the highly symmetrical sulfur hexafluoride[22] and tellurium hexafluoride[23,24] molecules, benzene,[25] acetonitrile,[26] and C_{60}[27] have been reported. Nanoparticles have high surface-to-volume ratios which can affect their physical and chemical behavior. Size dependences of electron delocalization, band gaps,[28] specific heats,[29] and melting points[30–33] are characteristic of nanoparticles.

The melting of nanoparticles of nitromethane is the focus of this work. A partially melted one-component nanoparticle of sufficient size (in the range of hundreds of molecules) is composed of a solid core in contact with a liquid shell through a surface of area a. If this nanoparticle is sufficiently large, a general thermodynamic analysis is valid. The Gibbs free energy of the solid (s), liquid (ℓ), and surface (σ) phases of the nanoparticle, respectively, are given by[34]

$$\begin{cases} \delta G^s = -S^s \delta T^s + v^s \delta P^s + \mu^s \delta n^s, \\ \delta G^\ell = -S^\ell \delta T^\ell + v^\ell \delta P^\ell + \mu^\ell \delta n^\ell, \\ \delta G^\sigma = -S^\sigma \delta T^\sigma - a\,\delta\gamma + \mu^\sigma \delta n^\sigma; \end{cases} \tag{1}$$

where γ is the solid–liquid surface tension and the other quantities have their usual thermodynamic meanings. The analog of the Gibbs–Duhem equation can be written for each phase,

$$\begin{cases} n^s \delta\mu^s + S^s \delta T^s - v^s \delta P^s = 0, \\ n^\ell \delta\mu^\ell + S^\ell \delta T^\ell - v^\ell \delta P^\ell = 0, \\ n^\sigma \delta\mu^\sigma + S^\sigma \delta T^\sigma - a\,\delta\gamma = 0. \end{cases} \tag{2}$$

This gives a total of $3\times 2=6$ independent intensive variables or degrees of freedom for the partially melted nanoparticle. The condition of heterogeneous equilibrium between the phases imposes the set of four extra restrictions, namely, $\mu^s = \mu^\ell = \mu^\sigma$, and $T^s = T^\ell = T^\sigma$. As a result, a nanoparticle solid core in equilibrium with a melted surface shell will have two remaining degrees of freedom, whereas the phase rule for bulk phases, where surface effects are neglected, allows only a single degree of freedom for a solid in equilibrium with a liquid. The two degrees of freedom for solid and liquid states in a nanoparticle show that at a given pressure, unlike bulk phases, a nanoparticle can have a solid–liquid-phase equilibrium (i.e., a melting transition) over a range of temperatures. For larger nanoparticles where a classical thermodynamic description remains valid a *surface premelting* model describes the change in melting point with nanoparticle size. In this mechanism, melting first occurs in the surface overlayer to form a liquid outer shell of thickness t_0. As the temperature rises, the liquid layer quickly expands into the core until the entire nanoparticle melts at the melting point, T_m. For this range of sizes, the variation of the melting point of the nanoparticle with radius r is given by[8,35,36]

$$T_0 - T_m = \frac{2T_0}{\Delta\mu_0^{\ell s}}\left[\frac{\gamma_{s\ell}}{\rho_s (r-t_0)} + \frac{\gamma_{\ell g}}{r}\left(\frac{1}{\rho_s} - \frac{1}{\rho_\ell}\right)\right], \tag{3}$$

where T_0 is the bulk melting temperature, $\Delta\mu_0^{\ell s}$ is the latent heat of fusion of the bulk solid, $\gamma_{s\ell}$ and $\gamma_{\ell g}$ are the solid–liquid and liquid–vapor surface tensions, respectively, and ρ_s and ρ_ℓ are the bulk solid and liquid densities, respectively.

[a]Electronic mail: alavi@chem.okstate.edu
[b]Electronic mail: dlt@okstate.edu

The adjustable parameter t_0 is the critical thickness of the liquid layer, above which the nanoparticle is considered melted.

A comprehensive set of studies of the physical properties of nanoparticles too small to be subject to macroscopic thermodynamic analysis have been carried out over the past two decades by Berry and co-workers.[24,37–42] Melting is one of the most studied and best characterized processes in nanoparticles. In small nanoparticles, the surface and core atoms are not distinct, and liquid and solid phases of the nanoparticle are in dynamic equilibrium rather than in coexistence. Only the solid form is stable for temperatures lower than T_f and only the liquid form is stable for temperatures higher than T_m. At temperatures between T_f and T_m the nanoparticle fluctuates between the solid and liquid states, much like the equilibrium between two chemical isomers. The ratio of the two states in an ensemble is given by $K=[\text{solid}]/[\text{liquid}]=\exp(-\Delta G/kT)$, where ΔG is the free energy difference between the solid and liquid forms of the nanoparticle. This mechanism is called *dynamic coexistence melting*.

In an early study, Berry, Jellinek, and Natanson[37] used a quantum statistical mechanical model to describe the solid to liquid transition in nanoparticles. They used a rigidity factor γ to characterize the rigid solid form ($\gamma=1$) and ''floppy'' nonrigid liquid form ($\gamma=0$) of the nanoparticles. In the range of temperatures between T_f and T_m the partition function, $Z(\gamma,T)$, of the nanoparticle has a minimum at intermediate values of γ. Between these temperatures the solid and liquid forms of the nanoparticle dynamically coexist. These model calculations were explicitly illustrated for a five-body cluster.

Dynamic coexistence melting is now well understood in terms of the minima of the potential energy surfaces of nanoparticles.[38–41] The free energy difference, ΔG, between the low-potential energy solid and high-potential energy liquid configurations of the nanoparticle determines the dynamic equilibrium between these two states. For rare-gas nanoparticles, the stability of solid configurations with ''magic numbers'' of atoms results in nonmonotonic variation of the melting point with the nanoparticle size.[38] The dynamic coexistence melting is displayed for rare-gas clusters with 19 or less atoms[38] and in a separate study for Lennard-Jones clusters with 55 and 147 particles.[43] This type of transition is considered to be a first-order phase transition broadened by finite size effects.[43] A statistical mechanical analysis based on a model partition function for a low-energy nanoparticle geometry (solid) in equilibrium with various higher energy geometries (liquid configuration) has also been used to illustrate the coexistence of the two phases and the observation of different freezing and melting points for different sized particles.[44]

Shi[33] has presented a general microscopic model that describes the size dependence of the melting point of nanoparticles based on the magnitudes of atomic thermal vibrations. The model is based on the Lindemann criterion for melting[45] and states that the ratio of the melting point of a nanoparticle with radius r to the melting point of a bulk liquid surface, $T_m(r)/T_m(\infty)$, is given by

$$\frac{T_m(r)}{T_m(\infty)}=\exp\left[\frac{-(\alpha-1)}{(r/3h-1)}\right], \tag{4}$$

where $\alpha=\sigma_s/\sigma_v$, σ_s^2, and σ_v^2 are, respectively, the mean-square deviation of the positions of the surface and the bulk molecules from their positions at the beginning of the simulation. The factor h corresponds to an approximate height of a monolayer of molecules on the bulk crystal surface. According to the analysis given by Shi,[33] nanoparticles with a diameter larger than $6h$ can retain their crystal structure, while smaller particles cannot.

Equations (3) and (4) assume a monotonic decrease of the melting point with nanoparticle size. Studies of the size dependence of melting points of Lennard-Jones[46,47] particles (up to 60 atoms) and sodium particles[11–13,48] (up to 200 atoms) show that the melting point varies in a nonmonotonic manner as the size of the particle decreases. These observations have been related to geometrical and electronic shell effects in these particles.[48]

Zhao *et al.*[32] have performed molecular-dynamics simulations of the melting of silver particles with 13 to 3871 atoms interacting with an embedded-atom model (EAM) potential. For large nanoparticles ($N=258-3871$), with radii greater than a critical value r_c, they observe surface premelting, whereas for nanoparticles in the size range $N=13-116$, dynamic coexistence melting is observed. The size range of dynamic coexistence is comparable to the rare-gas nanoparticles. An *intermediate melting mechanism* is observed for nanoparticles with $N\sim 120-240$ where the change in T_m with particle size is much slower than the surface pre-melting and dynamic coexistence melting regions. The latent heat of melting for clusters of this size is significantly greater than for clusters of the size where surface pre-melting and dynamic coexistence melting occurs.[32] The state of nanoparticles in this size range in the melting region can be described as slush-like.[38]

The melting transition in nanoparticles has been characterized by calculating various dynamic or structural properties of the nanoparticle at different temperatures. These properties include the Lindemann index[10,42,49] and root-mean-square bond length fluctuations.[38] Structural properties including the static structure factors,[32] radial distribution functions, and many different types of energy-temperature or heat capacity-temperature plots have also been used.[10,25,32,38,42,49–51] In this work we have used a set of properties to identify the melting transition in nanoparticles of nitromethane. These structural properties include the radial distribution functions, the nanoparticle core density, the dipole–dipole correlation function, and the diffusion coefficient. The melting regions obtained from these different properties are consistent with one another and indicate that the melting points of the clusters have been correctly identified.

We are interested in the structural and dynamical properties of molecular nanoparticles high-energy molecular compounds that may affect their chemical behavior; however, because relatively little is known about the fundamental properties of these molecular nanoparticles, we begin by examining some important physical properties and processes as

functions of particle size and temperature. For our initial study we have chosen nitromethane as representative of molecules with large dipole moments. We have used molecular-dynamics (MD) simulations to study solid and liquid properties of nanoparticles of 480, 240, 114, 96, 48, and 32 molecules of nitromethane. We have calculated the carbon–carbon radial distribution function, dipole–dipole correlation function, core density, interatomic enthalpy, and atomic diffusion coefficients as functions of the temperature to characterize the phase and thus the melting transitions of the particles.

This work continues a series of studies in which we are developing potentials and carrying out simulations to study the fundamental behavior of nitromethane,[52–54] which is part of a larger effort to develop accurate simulation methods generally applicable to nitro and nitramine energetic materials.[55] In our initial study of nitromethane, we developed a crystal model that accurately reproduces the unit cell parameters over a wide temperature range.[52] That flexible force field model has been shown to accurately predict liquid state properties.[53] Recently, we have used it, with slight modifications, to study the solid-to-liquid transition.[54] In the present work we use the modified force field model[54] to study the properties of nanoparticles as functions of size and temperature. The ultimate goal of these studies is to simulate reactive nitromethane nanoparticles and therefore we have included intramolecular motions although this is probably not necessary for simulations of the physical properties of nitromethane nanoparticles.

The nitromethane molecule is highly polar (3.46 D) and its physical and chemical properties have been well studied in bulk phases.[52] X-ray crystal structure analysis of nitromethane shows that between 4.2 and 228 K, crystalline nitromethane has the orthorhombic space group $P2_12_12_1$ with four molecules per unit cell[54,56,57] ($Z=4$). The melting point is 244.73 K.[58] We use bulk solid and liquid properties as references for nanoparticles properties that are calculated in this work.

A description of the inter- and intra-molecular force fields for nonreactive nitromethane molecules and the details of the molecular dynamics (MD) method used to study nitromethane nanoparticles are given in Sec. II. The results of the MD calculations for various sizes of nanoparticles at various temperatures are used to obtain structural and thermodynamic quantities, which are presented and interpreted in Sec. III. A summary and the conclusions of the study are given in Sec. IV.

II. THEORETICAL METHODS

A. The force field

The intramolecular force field used for nitromethane was developed by Sorescu *et al.*[52] with minor modifications by Agrawal *et al.*[54] This potential accurately predicts experimental solid[52] and liquid[53] state properties of nitromethane as well as the correct melting point behavior.[54] The intramolecular potential has the functional form:

$$V_{\text{intra}}=V_{\text{stretch}}+V_{\text{bend}}+V_{\text{torsion}}. \tag{5}$$

The bond stretch potentials are described by the Morse function

$$V_{\text{stretch}}=\sum_{i=1}^{6} D_{ei}\{[1-\exp(-\beta_i(r_i-r_i^0))]^2-1\}, \tag{6}$$

where r_i is the length of bond i in the molecule; the angle bending potentials are taken to be harmonic,

$$V_{\text{bend}}=\sum_{i=1}^{9} \frac{1}{2}k_i(\theta_i-\theta_i^0)^2, \tag{7}$$

and the torsional potential is a sum of cosine terms

$$V_{\text{torsion}}=\sum_{i=1}^{7} V_{\Phi i}[1+\cos(m_i\Phi_i-\delta_i)]. \tag{8}$$

The nine bending potentials correspond to the HCH (three), HCN (three), CNO (two), and ONO (one) angles. The seven terms in the torsional potential Eq. (8) correspond to the relative positions of the C–NO_2 atoms (one) and the orientations of the H atoms relative to the C–N–O planes (six). The values of the parameters in Eqs. (6)–(8) used in this work are given in Table I of Ref. 54. These parameters were determined by fitting the potential to geometrical parameters and normal mode frequencies of nitromethane determined from quantum chemistry calculations at the B3LYP/6-31G(d) level.[52]

The intermolecular potential is a superposition of Buckingham and Coulombic terms

$$V_{\alpha\beta}^{\text{inter}}(r)=A_{\alpha\beta}\exp(-B_{\alpha\beta}r)-\frac{C_{\alpha\beta}}{r^6}+\frac{q_\alpha q_\beta}{4\pi\epsilon_0 r}, \tag{9}$$

where r is the interatomic distance between atoms α and β on two different molecules and q_α and q_β are the electrostatic charges on these atoms. The values of the Buckingham coefficients $A_{\alpha\beta}$, $B_{\alpha\beta}$, and $C_{\alpha\beta}$ are those developed in crystal packing studies of hexahydro-1,3,5-trinitro-1,3,5-*s*-triazine (RDX).[59] It was found that these parameters are transferable to other high-energy nitro-compounds, including nitromethane.[60] The details regarding the assigning of electrostatic charges on the atoms are given in Ref. 52.

The lattice constants of the solid phase, average orientational parameters of the four nitromethane molecules in the unit cell, and the pressure variance of the unit cell dimensions calculated from this force field were compared to experimental values, with differences that are generally smaller than 3%.[52] This force field has been used to calculate the liquid-state density, enthalpy of vaporization, diffusion coefficient, and shear viscosity, with generally quite good agreement with experimental results.[52] Agrawal *et al.*[54] used this potential to determine the melting point of nitromethane by studying the equilibrium coexistence temperature of solid and liquid nitromethane in a constant energy MD simulation. The predicted melting point of 255.5 K is in good agreement with the experimental melting point of 244.73 K.

B. Molecular dynamics calculations

In the present study, molecular-dynamics calculations on solid and liquid nitromethane and nitromethane nanoparticles

were done for the DL_POLY 2.12 program.[61] Solid and liquid calculations were done with the NPT ensemble at 1 atm pressure and with periodic boundary conditions, applying a Nosé–Hoover thermostat–barostat[62–64] with relaxation times for the temperature and pressure of 0.1 and 2.0 fs, respectively. The Verlet leapfrog scheme[64,65] was used to time integrate of the equations of motion. Ewald's method[64] was used to deal with long-range electrostatic forces. A 5×4×3 supercell, which contains 240 nitromethane molecules was used in the solid-state simulations. This gives a nearly cubic simulation box with dimensions 26.22 Å×25.28 Å×26.19 Å. The NPT barostat routine allows a homogenous expansion or contraction of the sides of this supercell. Liquid-state simulations were initiated in a cubic box 26.22 Å on each side. A total of 216 molecules were placed inside the liquid simulation box, which are ~10% fewer molecules than in the solid-state simulation box of similar dimensions. In the solid-state calculations, a time step of 0.75 fs was used and trajectories were carried out for a total of 37.5 ps, with the first 3.75 ps used to equilibrate the system. A time step of 0.5 fs was used in the liquid-state calculations, which require a much run longer times to converge and were thus propagated for a total of 150 ns time steps with the first 50 ns being for equilibration.

Simulations of the nanoparticles were done with the NVT ensemble with no periodic boundary conditions. These simulations mimic the formation of nanoparticles from solidlike fragments under adiabatic, low-pressure conditions. A time step of 0.5 fs was used, and the total duration of the nanoparticle simulations was 75 ps, with the first 25 ps used for equilibration. Electrostatic forces were calculated directly for the finite nanoparticles. Six sets of nanoparticle simulations with 480, 240, 144, 96, 48, and 32 nitromethane molecules were performed. The initial geometries of these nanoparticles corresponds to capped supercells of solid nitromethane at 4.2 K; for example, 480-, 240-, and 96-molecule nanoparticles correspond to capped 6×5×4, 5×4×3, and 4×3×2 supercells. The initial structures used in these simulations were highly symmetric and simulations were not begun from optimal, lowest-energy configurations at each nanoparticle size. We assume that simulations with these highly symmetric initial states converge to the putative global minimum at each temperature. Simulations on strongly hydrogen-bonded water[17] and ionized water[18] nanoparticles indicate that the melting point of the nanoparticle does not depend on the initial configuration, and therefore, the same general global minimum structure is reached from different initial configurations. We assume the same behavior to hold for nitromethane. Given the strong intermolecular bonding and nonspherical shapes of the nitromethane molecules, the minimum energy configurations for nanoparticles of this material will be much more difficult to determine (both theoretically and experimentally) than the case of Lennard-Jones nanoparticles. Configurations obtained after a reasonable equilibration time should thus be comparable in energy and have similar solid–liquid transition temperatures.

All interatomic interactions were determined for the atoms in the simulation within a cutoff distance of R_{cutoff}. For the largest nanoparticle, the value $R_{\text{cutoff}}=13.0$ Å was used.

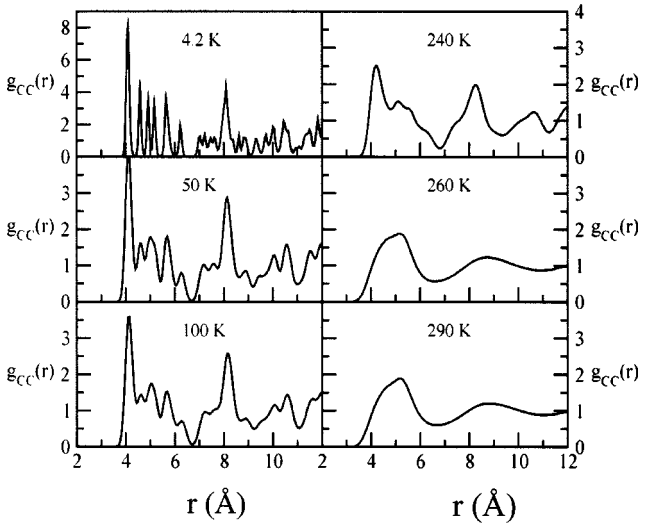

FIG. 1. The carbon–carbon radial distribution functions of bulk nitromethane at solid and liquid temperatures. The experimental melting point of nitromethane is 244.7 K. The change of phase is apparent from the disappearance of long-range structure and the broadening of peaks for the first and second coordination shells in the solid (e.g., compare the curves for $T=240$ K and $T=260$ K).

The cutoff distance was adjusted appropriately for the smaller nanoparticles. Given the strong intermolecular forces in the Hamiltonian, evaporation of the nanoparticles was not observed in the range of temperatures studied and it was not necessary to confine nanoparticles within a simulation box to prevent loss of molecules through evaporation.

III. RESULTS

Solid- and liquid-state simulations were performed to provide reference values for the physical properties of the nanoparticles. The structures of the solid and liquid phases are characterized at various temperatures by the carbon–carbon radial distribution function of nitromethane

$$g_{CC}(r)=\frac{1}{nN}\left\langle \sum_i \sum_j \delta[r-r_{ij}]\right\rangle, \tag{10}$$

where N is the total number of carbon atoms (or nitromethane molecules), n is the number density, and r_{ij} is the separation between carbon atoms i and j. The computed carbon–carbon radial distribution functions for $T=4.2$, 50, 100, 240, 260, and 290 K are shown in Fig. 1. Note that there is some variation in the scales of the y-axes because of variations in the intensities. The long-range correlations in the solid phase are apparent from the many peaks in $g_{\text{CC}}(r)$ at temperatures up to 240 K. As the temperature is increased, the vibrational motion of the carbon atoms broadens the peaks in the $g_{\text{CC}}(r)$ curves. The locations of the peaks, which correspond to the average separation of the atoms, do not change, indicating fixed positions in a crystal structure. In the liquid phase the long-range correlations are lost and the positions of the maxima, which represent the locations of the neighboring correlation shells, are shifted relative to those for the solid (see the plots for 260 and 290 K in Fig. 1).

Nanoparticles of 480, 240, 144, 96, 48, and 32 nitromethane molecules were studied over the temperature

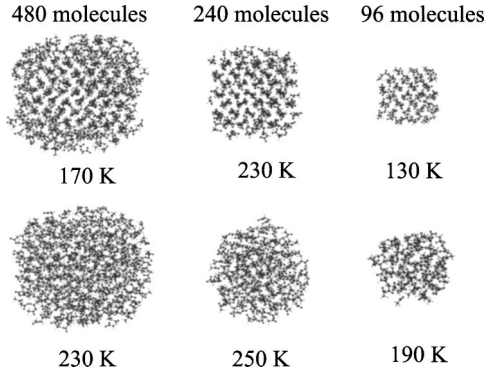

FIG. 2. Sample configurations for 480-, 240-, and 96-molecule nitromethane nanoparticles. The top row are structures for temperatures at which the core of the nanoparticle remains solid, although significant surface rearrangement has occurred. The structures in the bottom row are for temperatures at which the nanoparticles have melted.

range 50–290 K. Sample configurations for solid and liquid nanoparticles of 480, 240, and 96 molecules are shown in Fig. 2. The top row of this figure shows ''snapshots'' of solid-state nanoparticles where the ordered structure of the core is apparent but extensive surface relaxation has occurred. Liquid nanoparticles, which have attained near-spherical shapes, are shown in the bottom row of Fig. 2; these are results of simulations of 75 ps duration.

The retention of crystallographic structure in the nanoparticles can be quantitatively characterized by the carbon–carbon radial distribution function. The radial distribution functions for the 480-, 240-, 144-, and 96-molecule nanoparticles for the structures are shown in Fig. 3. A low-temperature solid structure and a liquid nanoparticle structure are given for each nanoparticle. The general locations of the main peaks in the carbon–carbon radial distribution function for the nanoparticles correspond with the locations of the peaks of solid and liquid bulk nitromethane shown in Fig. 1. In the solid state, the radial distance of the first two main neighboring shells in the nanoparticles are ~4 and 8 Å from

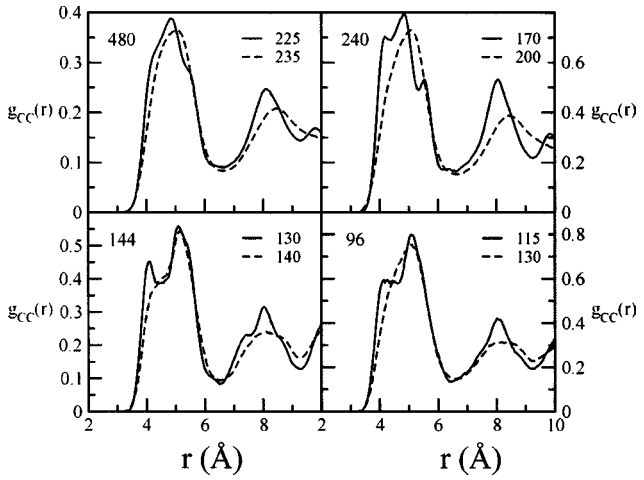

FIG. 3. The carbon–carbon radial distribution functions, $g_{CC}(r)$, for the 480-, 240-, 144-, and 96-molecule nitromethane nanoparticles at one temperature before melting (solid lines) and one temperature after melting (dashed lines). The melting transition is seen in the destruction of long-range order and the outwards shift of the peaks for the nearest neighbor shells.

each carbon (see Fig. 1). These distances correspond to the largest peaks in solid nitromethane nanoparticles in Fig. 3. In the bulk liquid, the location of the nearest neighbor shells are shifted outwards to about 5 and 8.7 Å, as is seen in Fig. 1. A corresponding shift is observed for the liquid nanoparticles in Fig. 3. For the 480-molecule nanoparticle shown in Fig. 3, the $g_{CC}(r)$ curve at 225 K shows the detailed, long-range structure that is characteristic of the solid. At 235 K, the locations of the first and second maxima of the $g_{CC}(r)$ have shifted outwards as the nanoparticle melts. Similar qualitative changes in $g_{CC}(r)$ begin near 180 K for the 240-molecule nanoparticle, at 135 K for the 144-molecule nanoparticle, and at about 120 K for the 96-molecule nanoparticle. The carbon–carbon radial distribution functions of the 48- and 32-molecule nanoparticles (not shown) display similar qualitative behavior. The results in Fig. 3 show that melting of the nanoparticles occurs at temperatures lower than bulk nitromethane (244 K) and that the melting depends on the size of nanoparticle. The smaller nanoparticles have lower melting points. The dependence of the melting point on nanoparticle size and the range of melting of the nanoparticle have been predicted from thermodynamic analysis of surface effects[30,31,33] and has been experimentally observed in gold[6] and cadmium sulfide[14] and many other nanoparticle systems.

The radial distribution functions give only spatial information about the distribution of the carbon atoms in the nanoparticles. Information about the relative orientations of the nitromethane molecules at different temperatures in bulk phases and nanoparticles can be obtained by calculating the ensemble average dipole–dipole correlation function, $\langle \cos\theta(R_{\mathrm{cm-cm}})\rangle$,

$$\langle \cos\theta(R_{\mathrm{cm-cm}})\rangle = \langle \mathbf{s}_i \cdot \mathbf{s}_j \rangle, \tag{11}$$

where $\mathbf{s}_i$ is the unit vector in the direction of the dipole moment $\boldsymbol{\mu}_i$, of molecule i,

$$\mathbf{s}_i = \frac{\boldsymbol{\mu}_i}{|\boldsymbol{\mu}_i|}. \tag{12}$$

The brackets $\langle\ \rangle$ in Eq. (11) represent an average over all pairs i and j, and also an average over the time of the simulation. $R_{\mathrm{cm-cm}}$ represents the separation of the centers-of-mass of nitromethane pairs i and j. The dipole–dipole correlation functions for the 480-molecule nanoparticle at different temperatures between 190 and 275 K are shown in Fig. 4, where the same function for liquid nitromethane at 290 K is given for comparison. In all cases, strong dipole–dipole interactions cause the dipole moment vectors of the nearest-neighbor molecules (with center-of-mass separations between 3 and 4 Å) to be arranged in an antiparallel manner ($\cos\theta<0$). For the solid nanoparticle at 190 K, dipole–dipole correlations remain strong over long distances, which parallels the long-range correlations in the radial distribution function of the solid (see Figs. 1 and 3). In the liquid nanoparticle at 235 K and the bulk liquid, most dipole correlations beyond the second shell of neighbors are negligible. The fact that the shape of the dipole correlation curves show large qualitative changes within a small temperature range that corresponds exactly with the temperature range where

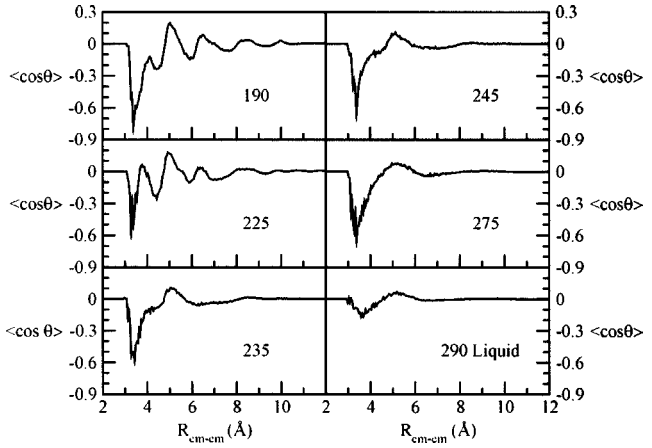

FIG. 4. The ensemble average dipole–dipole correlation function as a function of distance from the center of mass of two nitromethane molecules for the 480-molecule nanoparticle at different temperatures. The dipole–dipole correlation function of the liquid at 290 K is given for comparison. The long-range correlations up to 225 K indicate that the dipoles are strongly correlated up to this temperature, whereas only correlations between close neighboring molecules are present in the melted nanoparticle at 235 K and above and also in the liquid.

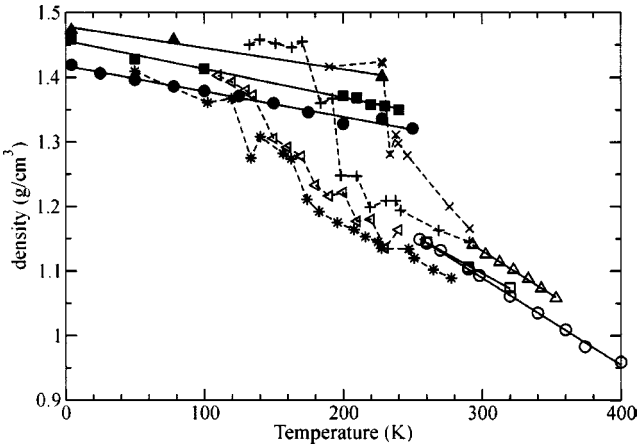

FIG. 5. Variation of density with temperature for solid nitromethane calculated in this work (■), from experiment (▲) and by Sorescu *et al.* (Ref. 51) (●); liquid nitromethane from the present work (□), experiment (△), and the simulations of Sorescu *et al.* (Ref. 52) (○); the 480-molecule (×), the 240-molecule (+), the 144-molecule (◁), and the 96-molecule nanoparticle (*) of nitromethane. The melting transition is manifested by the region of the sharp drop in the density. The nanoparticles melt over a finite region of temperature. The melting occurs at lower temperatures as the size of the nanoparticle decreases. The high density of the solid phases of the 480- and 240-molecule nanoparticles is a result of the way density is defined for the nanoparticle as explained in the text.

large changes are seen in the radial distribution function provides further independent evidence of melting of the nanoparticles.

A quantitative determination of the melting point T_m for the nanoparticles could be based on radial distribution functions, such as shown in Fig. 3; however, it is more straightforward to use other properties which can be quantitatively determined to characterize the nanoparticles at different temperatures. At the experimental melting point of nitromethane, 244.73 K,[56] a discontinuity in density is observed which is reproduced in simulations[54] and shows the first-order nature of the phase transition. The calculated bulk solid (■) and liquid densities (□) of nitromethane at different temperatures are shown in Fig. 5 along with experimental solid (▲) and liquid (△) data, and previous simulation results for the solid (●)[52] and liquid (○).[53] The melting of bulk nitromethane has been studied by Agrawal *et al.*[54] They found that the change in density is an accurate indicator of the melting transition.

The density of a nanoparticle is not a well-defined quantity because a unique outer boundary for the nanoparticle does not exist. A similar problem is encountered in studying the evaporation of liquid droplets.[66] A dividing surface (i.e., Gibbs surface[34]) for a liquid droplet in equilibrium with the vapor phase has been used to determine the density of the droplet.[66] In this study, an average core density of a nanoparticle is calculated in a heuristic manner. A sphere, called the reference sphere, with its origin at the center of mass of the nanoparticle, is drawn with a minimum radius of 10 Å. The core density of the nanoparticle is defined by determining the mass of the total number of molecules inside the volume of this sphere. The location of the center-of-mass of each molecule determines whether it is counted inside the reference sphere. The radius of the reference sphere is increased by increments and the density at each radius is determined. As the radius of the reference sphere becomes larger than the ''outer boundary'' of the nanoparticle, the densities calculated in this manner begin to decay because the volume of the reference sphere increases without a proportional increase in the number of nitromethane molecules. The density of the 480-molecule nanoparticle begins to diminish as the radius of the reference sphere exceeds 15 Å. The density of the 480-molecule nanoparticle at different temperatures is therefore averaged over reference spheres with radii between 10 and 15 Å.

The computed densities of the 480- (×), 240- (+), 144- (◁), and 96-molecule (*) nanoparticles at various temperatures are shown in Fig. 5. The drop in the density as temperature increases characterizes the melting transition. The density drop for the smaller nanoparticles occurs at lower temperatures and also over a larger temperature range. The densities of the nanoparticles shown in Fig. 5 converge to the liquid-state value at high temperatures. The results in Table I show the variation of the density with temperature for the 480-, 240-, 144-, and 96-molecule nanoparticles. The small size of the 48- and 32-molecule nanoparticles precludes determining a well-defined core density for them in this manner.

A discontinuity is also seen in the temperature behavior of the values of the enthalpy of sublimation of solid nitromethane and enthalpy of vaporization of liquid nitromethane as the temperature passes through the melting point (see Fig. 6). The enthalpies of sublimation and vaporization are defined in a similar manner for the solid and liquid phases

$$\Delta H_{\mathrm{sub}} = -U_{\mathrm{int}} + RT, \tag{13}$$

$$\Delta H_{\mathrm{vap}} = -U_{\mathrm{int}} + RT, \tag{14}$$

where in the present simulations the internal energy (i.e., the

TABLE I. Core density (g/cm^3) of nitromethane in the solid, liquid, and nanoparticles of 480-molecules, 240-molecules, 144-molecules, and 96-molecules at various temperatures (K).

T	ρ_{solid}	T	ρ_{liquid}	T	ρ_{480}	T	ρ_{240}	T	ρ_{144}	T	ρ_{96}
4.2	1.459	250	1.155	190	1.42	132	1.42	102	1.37	50	1.41
50	1.428	260	1.145	228	1.42	140	1.46	112	1.40	102	1.36
100	1.413	290	1.106	229	1.42	151	1.45	123	1.39	120	1.37
200	1.371	298	1.098	234	1.28	163	1.45	134	1.38	134	1.28
210	1.368	320	1.074	238	1.31	171	1.46	136	1.37	140	1.31
220	1.358			240	1.30	184	1.36	143	1.31	157	1.28
230	1.356			246	1.28	192	1.37	151	1.30	163	1.27
240	1.350			276	1.20	198	1.25	166	1.29	174	1.21
				291	1.17	210	1.24	171	1.28	183	1.19
						219	1.20	182	1.23	196	1.18
						231	1.21	197	1.22	208	1.16
						238	1.21	201	1.22	216	1.15
						241	1.19	214	1.18	225	1.14
						269	1.16	220	1.18	228	1.14
						291	1.14	234	1.16	247	1.13
								241	1.16	251	1.20
										265	1.10
										278	1.09

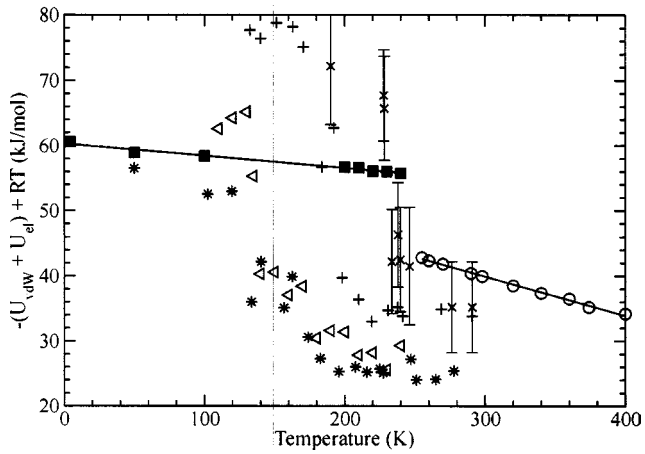

FIG. 6. The variation of the enthalpy of sublimation and vaporization of solid, and liquid nitromethane and $-(U_{vdW}+U_{el})+RT$ for nitromethane nanoparticles with temperature. The symbols used are the same as in Fig. 6. Error bars are given for the 480-molecule nanoparticle. These error bars, obtained from the MD calculations, are typical of the uncertainties in the values of the enthalpy for the other nanoparticles.

intermolecular interaction energy) U_{int} is the sum of the van der Waals (vdW) and electrostatic interactions between the molecules; $U_{int}=U_{vdW}+U_{el}$.

The melting transition of the nanoparticle can also be characterized by the temperature variation of the intermolecular enthalpy. The enthalpies corresponding to $\Delta H^*_{int}=-(U_{vdW}+U_{el})+RT$ for the 480- ($\times$), 240- ($+$), 144- ($\lhd$), and 96-molecule (*) nanoparticles are shown in Fig. 6 along with the solid- and liquid-state values. Error bars are shown on the values of the enthalpy for the 480-molecule nanoparticle at various temperatures. The enthalpies of the other nanoparticles have similar uncertainties. The values of the enthalpies show a drop at the melting temperature. For larger nanoparticles, this drop occurs at higher temperatures, which approach the melting point of the bulk phase. Whereas the drop in $-(U_{vdW}+U_{el})+RT$ with temperature for bulk phases is sharp at the melting point, this drop occurs over a range of temperatures for the nanoparticles, which corresponds to the melting range of the nanoparticle. As in the case of density (see Fig. 5), the drop in the enthalpy occurs at lower temperatures for the smaller nanoparticles. The values of ΔH^*_{int} for the various sizes of nanoparticles are given in Table II. The fluctuations in energy of the 48- and 32-molecule nanoparticle are large and thus well-defined values of ΔH^*_{int} are difficult to obtain.

The density and enthalpy curves in Figs. 5 and 6, respectively, indicate the same temperature range for melting for each of the nanoparticles. This range also corresponds to the temperatures where qualitative changes begin to appear in the radial distribution function curves for the nanoparticles shown in Fig. 3. To further verify that the transitions observed in Figs. 3, 5, and 6 represent melting and not a plastic

TABLE II. The enthalpy (kcal/mol) of sublimation ΔH_{sub} of solid nitromethane, of vaporization ΔH_{vap} of liquid nitromethane, and the intramolecular enthalpy ΔH^*_{int} of nanoparticles at various temperatures (K).

T (K)	ΔH_{sub}	T	ΔH_{vap}	T	$\Delta H^*_{int}(480)$	T	$\Delta H^*_{int}(240)$	T	$\Delta H^*_{int}(144)$	T	$\Delta H^*_{int}(96)$
4.2	60.58	250	44.76	190	72	132	78	102	57	50	56
50	58.90	260	44.32	228	68	140	76	112	62	102	52
100	58.37	290	42.66	229	66	151	79	123	64	120	53
200	56.69	298	42.73	234	42	163	78	134	65	134	36
210	56.58	320	41.56	238	46	171	75	136	55	140	42
220	56.05			240	42	184	57	143	40	157	35
230	56.00			246	42	192	63	151	41	163	40
240	55.72			276	35	198	40	166	37	174	31
				291	35	210	36	171	38	183	27
						219	33	182	30	196	25
						231	35	197	32	207	26
						238	35	201	31	216	25
						241	34	214	28	225	26
						269	35	220	28	228	25
						291	34	234	26	247	27
								241	29	251	24
										265	24
										278	25

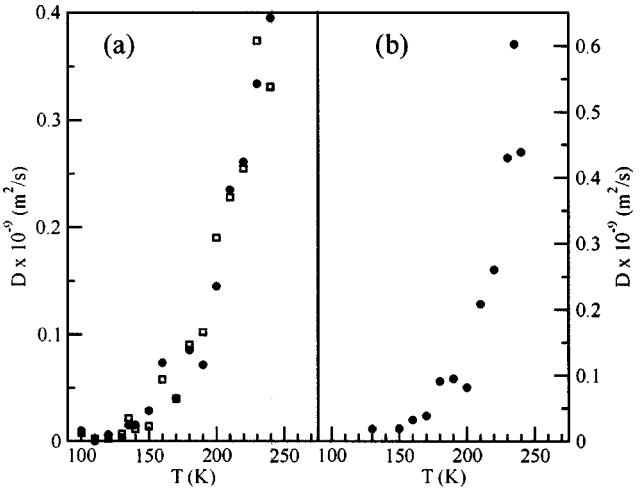

FIG. 7. The variation of the diffusion coefficient for carbon (●) and nitrogen (□) atoms with temperature for the 144-molecule (a) and the 240-molecule nanoparticle (b). The diffusion coefficients show a rise of more than an order of magnitude in the melting region. The region of rapid increase corresponds to the predicted melting points from the other characterization methods shown in the previous figures.

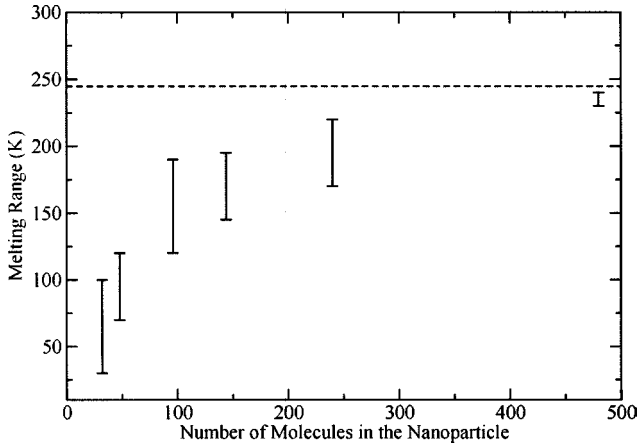

FIG. 8. The melting range (in Kelvin) as a function of the number of nitromethane molecules in the nanoparticle. The asymptotic value of 244.73 K for the experimental melting point of bulk nitromethane is shown by the dashed line.

phase transition, the diffusion coefficients calculated for the carbon and nitrogen atoms in the 144- and 240-molecule nanoparticles at different temperatures are shown in Fig. 7. There is an order of magnitude increase in the diffusion coefficients in the nanoparticles over a short range of temperature. This corresponds to the melting of the nanoparticle in this temperature range. The temperature range of the sharp increase in diffusion coefficient for these two nanoparticles corresponds with the temperature ranges where the radial distribution function, density, dipole–dipole correlation, and enthalpy also show quantitative changes. These changes can thus be related to the melting process.

Together, these sets of data give us confidence that the temperature ranges of melting have been accurately determined. The ranges of melting temperatures for the various nanoparticles are given in Table III and plotted in Fig. 8. The melting point of the 480-molecule nanoparticle approaches the bulk value. For the 48- and 32-molecule nanoparticle, the melting ranges were determined solely by the changes in structure as evident in the carbon–carbon radial distribution function and thus are perhaps less well defined. The decrease in melting temperature with nanoparticle size appears monotonic. This is in contrast with the behavior of Lennard-Jones[38] and sodium[12,13] nanoparticles, which show nonmonotonic variations in the melting point due to magic-number effects in nanoparticles with complete shells. Nitromethane has a more complex geometrical structure, which will lead to a greater number of potential minima in the potential energy landscape of the nanoparticles. A more exhaustive set of calculations on smaller nanoparticles is needed to investigate magic-number effects in nitromethane nanoparticles.

TABLE III. The range of melting temperatures (K) determined from density, enthalpy of vaporization, and carbon-carbon radial distribution function results for nanoparticles of nitromethane with various numbers of molecules.

Number of molecules in the nanoparticle	Melting range
480	230–240
240	170–220
144	140–200
96	120–190
48	70–120
32	30–100

IV. SUMMARY AND CONCLUSIONS

Structure and physical properties of 480-, 240-, 144-, 96-, 48-, and 32-molecule nanoparticles of nitromethane have been studied at different temperatures with molecular-dynamics simulations using the force field of Sorescu, Rice, and Thompson,[52] as modified by Agrawal, Rice, and Thompson.[54] The selected physical properties of these materials have been compared with those for the bulk solid and liquid. The carbon–carbon radial distribution functions, densities, internal enthalpies, dipole–dipole correlation functions, and atomic diffusion coefficients are studied for the various cases. The melting transition for the nanoparticles is easily identified and occurs over a range of temperatures up to 70 K.

The changes in the structure of the radial distribution function (see Fig. 3), the density (see Fig. 5), the enthalpy of vaporization (see Fig. 6), and diffusion coefficient (see Fig. 7) with temperature all indicate that the melting point of nitromethane nanoparticles is size dependent with the smaller nanoparticles melting at lower temperatures than large nanoparticles. Melting of nanoparticles occurs over a temperature range, rather than at a single temperature, with the size of the range decreasing with increasing particle size. In the melting range, long-range structural features of the nanoparticle, related to the long-range order begin to disappear, while short-range structure is retained, as shown by the plots of the carbon–carbon radial distribution function shown in Fig. 3.

As discussed in the Introduction, three general mechanisms, i.e., surface premelting models for large nanopar-

ticles, dynamic coexistence melting for small nanoparticles, and intermediate melting have been proposed to describe the melting of nanoparticles composed of atoms.[32,38] The sizes of nanoparticles in the present study ($N=32-480$), span the range of all three mechanisms. A more detailed analysis of the microscopic structure, melting ranges, and enthalpy of melting of nitromethane nanoparticles at different temperatures will be required to determine the exact nature of the melting mechanisms for this molecular material.

The calculation of physical properties provides a basis for the study of chemical decompositions or other reactions of molecules in nanoparticles. The decomposition of a number of energetic materials (such as ammonium dinitramide and CL-20) occurs in the liquid state. A study of reactive nanoparticles of these materials can give an indication of whether the reactivity of these materials is enhanced at the lower temperatures where the smaller nanoparticles melt.

ACKNOWLEDGMENTS

This work was supported by the U.S. Army Research Office under Grant No. DAAD19-01-1-0503. We are grateful to Dr. Paras M. Agrawal for several fruitful discussions.

[1] *Nanoscale Materials in Chemistry*, edited by K. J. Klabunde (Wiley, New York, 2001).
[2] H. Gleiter, Prog. Mater. Res. **33**, 223 (1989).
[3] J. A. Northby, J. Chem. Phys. **87**, 6166 (1987).
[4] D. Romero, C. Barron, and S. Gomez, Comput. Phys. Commun. **123**, 87 (1999).
[5] J. P. Doye and D. J. Wales, J. Chem. Phys. **102**, 9659 (1995); D. J. Wales and J. P. K. Doye, J. Phys. Chem. A **101**, 5111 (1997); J. P. K. Doye, D. J. Wales, and M. A. Miller, J. Chem. Phys. **109**, 8143 (1998).
[6] Ph. Buffat and J. P. Borel, Phys. Rev. A **13**, 2287 (1976).
[7] T. Castro, R. Reifenberger, E. Choi, and R. P. Andres, Phys. Rev. B **42**, 8548 (1990).
[8] S. L. Lai, J. Y. Guo, V. Petrova, G. Ramanath, and L. H. Allen, Phys. Rev. Lett. **77**, 99 (1996).
[9] H. Grönbeck, D. Tománek, S. G. Kim, and A. Rosén, Chem. Phys. Lett. **264**, 39 (1997).
[10] J. Westergren, S. Nordholm, and A. Rosén, Phys. Chem. Chem. Phys. **5**, 136 (2003).
[11] P. Kusche, Th. Hippler, M. Schmidt, B. von Issendorff, and H. Haberland, Eur. Phys. J. D **9**, 1 (1999).
[12] M. Schmidt, Th. Hippler, J. Donges, W. Kronmüller, B. von Issendorff, H. Haberland, and P. Labastie, Phys. Rev. Lett. **87**, 203402 (2001).
[13] M. Schmidt, J. Donges, Th. Hippler, and H. Haberland, Phys. Rev. Lett. **90**, 103401 (2003).
[14] A. N. Goldstein, C. M. Echer, and A. P. Alivisatos, Science **256**, 1425 (1992).
[15] A. P. Alivisatos, Science **271**, 933 (1996).
[16] D. J. Wales and I. Ohmine, J. Chem. Phys. **98**, 7245 (1993).
[17] A. V. Egorov, E. N. Brodskaya, and A. Laaksonen, J. Chem. Phys. **118**, 6380 (2003).
[18] E. N. Brodskaya, A. V. Egonov, A. P. Lyubartsev, and A. Laaksonen, J. Chem. Phys. **119**, 10237 (2003).
[19] T. Campbell, R. J. Kalia, A. Nakono, P. Vashishta, S. Ogata, and S. Rodgers, Phys. Rev. Lett. **82**, 4866 (1999); R. J. Kalia, T. Campbell, A. Chaterjee, A. Nakono, P. Vashishta, and S. Ogata, Comput. Phys. Commun. **128**, 245 (2000).
[20] S. Alavi, J. W. Mintmire, and D. L. Thompson (unpublished).
[21] G. Torchet, M.-F. de Feraudy, A. Boutin, and A. H. Fuchs, J. Chem. Phys. **105**, 3671 (1996).
[22] A. Boutin and A. H. Fuchs, J. Chem. Phys. **98**, 3290 (1993); A. Boutin, J.-B. Maillet, and A. H. Fuchs, *ibid.* **98**, 7245 (1993); G. Torchet, M.-F. Feraudy, B. Raoult, J. Farges, A. H. Fuchs, and G. S. Pawley, *ibid.* **92**, 6768 (1990).
[23] B. Chuko and L. S. Bartell, J. Phys. Chem. **97**, 9969 (1993).
[24] A. Proykova and R. S. Berry, Z. Phys. D: At., Mol. Clusters **40**, 215 (1997).
[25] G. Del Mistro and A. J. Stace, J. Chem. Phys. **98**, 3905 (1993).
[26] D. Wright and M. S. El-Shall, J. Chem. Phys. **100**, 3791 (1994).
[27] F. Calvo, J. Phys. Chem. B **105**, 2183 (2001).
[28] *Physics and Chemistry of Metal Cluster Compounds*, edited by J. de Jongh (Kluwer, Dordrecht, 1994).
[29] H. Y. Bai, J. L. Luo, D. Jin, and J. R. Sun, J. Appl. Phys. **79**, 361 (1996).
[30] H. Reiss and I. B. Wilson, J. Colloid Interface Sci. **3**, 551 (1948).
[31] R. E. Kunz and R. S. Berry, Phys. Rev. Lett. **71**, 3987 (1993).
[32] S. J. Zhao, S. Q. Wang, D. Y. Cheng, and H. Q. Ye, J. Phys. Chem. B **105**, 12857 (2001).
[33] F. G. Shi, J. Mater. Res. **9**, 1307 (1994).
[34] J. G. Kirkwood and I. Oppenheim, *Chemical Thermodynamics* (McGraw-Hill, New York, 1961).
[35] C. R. M. Wronski, Br. J. Appl. Phys. **18**, 1731 (1967).
[36] V. P. Skripov, V. A. Koverda, and V. N. Skokov, Phys. Status Solidi A **66**, 109 (1981).
[37] R. S. Berry, J. Jellinek, and G. Natanson, Phys. Rev. A **30**, 919 (1984).
[38] T. L. Beck, J. Jellinek, and R. S. Berry, J. Chem. Phys. **87**, 545 (1987).
[39] R. Kunz and R. S. Berry, Phys. Rev. E **49**, 1895 (1994).
[40] D. J. Wales and R. S. Berry, Phys. Rev. Lett. **73**, 2875 (1994).
[41] K. D. Ball, R. S. Berry, R. E. Kunz, F.-Y. Li, A. Proykova, and D. J. Wales, Science **271**, 963 (1996).
[42] A. Proykova, S. Pisov, R. Radev, P. Mihailov, I. Daykov, and R. S. Berry, Vacuum **68**, 87 (2003).
[43] P. Labastie and R. L. Whetten, Phys. Rev. Lett. **65**, 1567 (1990).
[44] M. Bixon and J. Jortner, J. Chem. Phys. **91**, 1631 (1989).
[45] F. A. Lindemann, Phys. Z. **11**, 609 (1910).
[46] D. J. Wales and R. S. Berry, J. Chem. Phys. **92**, 4283 (1990).
[47] D. D. Frantz, J. Chem. Phys. **115**, 6136 (2001).
[48] F. Calvo and F. Spiegelmann, J. Chem. Phys. **112**, 2888 (2000).
[49] W. D. Kristensen, E. J. Jensen, and R. M. J. Cotterill, J. Chem. Phys. **60**, 4161 (1974); C. L. Briant and J. J. Burton, *ibid.* **63**, 2045 (1975); R. D. Etters and J. B. Kaelberer, Phys. Rev. A **11**, 1068 (1975); J. B. Kaelberer and R. D. Etters, J. Chem. Phys. **66**, 3233 (1977); R. D. Etters and J. B. Kaelberer, *ibid.* **66**, 5112 (1977).
[50] P. Shah, S. Roy, and C. Chakravarty, J. Chem. Phys. **118**, 10671 (2003).
[51] T. Bachels, H. J. Güntherodt, and R. Schäfer, Phys. Rev. Lett. **85**, 1250 (2000).
[52] D. C. Sorescu, B. M. Rice, and D. L. Thompson, J. Phys. Chem. A **105**, 9336 (2001).
[53] D. C. Sorescu, B. M. Rice, and D. L. Thompson, J. Phys. Chem. A **104**, 8406 (2000).
[54] P. M. Agrawal, B. M. Rice, and D. L. Thompson, J. Chem. Phys. **119**, 9617 (2003).
[55] See Refs. 51–54 and references therein.
[56] S. F. Trevino, E. Prince, and C. R. Hubbard, J. Chem. Phys. **73**, 2996 (1980).
[57] V. M. Grosev, F. Stelzer, and D. Jocham, J. Mol. Struct. **476**, 181 (1999).
[58] W. M. Jones and W. F. Giauque, J. Am. Chem. Soc. **69**, 983 (1947).
[59] D. C. Sorescu, B. M. Rice, and D. L. Thompson, J. Phys. Chem. B **101**, 798 (1997).
[60] D. C. Sorescu, B. M. Rice, and D. L. Thompson, J. Phys. Chem. A **102**, 8386 (1998); **103**, 989 (1999).
[61] T. R. Forester and W. Smith, DL_POLY 2.0, CCLRC, Daresbury Laboratory, 1995.
[62] S. Nosé, J. Chem. Phys. **81**, 511 (1984).
[63] W. G. Hoover, Phys. Rev. A **31**, 1695 (1985).
[64] M. P. Allen and D. J. Tildesley, *Computer Simulation of Liquids* (Oxford Science Publications, Oxford, 1987).
[65] R. W. Hockney and J. W. Eastwood, *Computer Simulations Using Particles* (McGraw-Hill, New York, 1981).
[66] S. M. Thompson, K. E. Gubbins, J. P. R. B. Walton, R. A. R. Chantry, and J. S. Rowlinson, J. Chem. Phys. **81**, 530 (1984).